



HAL
open science

Exciton dynamics in droplet epitaxial quantum dots grown on (311)A oriented substrates

Marco Abbarchi, Takaaki Mano, Takashi Kuroda, Kazuaki Sakoda

► **To cite this version:**

Marco Abbarchi, Takaaki Mano, Takashi Kuroda, Kazuaki Sakoda. Exciton dynamics in droplet epitaxial quantum dots grown on (311)A oriented substrates. *Nanomaterials*, 2021, 10.3390/nano10091833 . hal-03602850

HAL Id: hal-03602850

<https://hal.science/hal-03602850>

Submitted on 9 Mar 2022

HAL is a multi-disciplinary open access archive for the deposit and dissemination of scientific research documents, whether they are published or not. The documents may come from teaching and research institutions in France or abroad, or from public or private research centers.

L'archive ouverte pluridisciplinaire **HAL**, est destinée au dépôt et à la diffusion de documents scientifiques de niveau recherche, publiés ou non, émanant des établissements d'enseignement et de recherche français ou étrangers, des laboratoires publics ou privés.

Article

Exciton dynamics in droplet epitaxial quantum dots grown on (311)A oriented substrates

Marco Abbarchi^{1,†,‡} , Takaaki Mano^{2,*} , Takashi Kuroda^{2,‡}  and Kazuaki Sakoda^{2,‡} ¹ Aix Marseille Univ, Universite de Toulon, CNRS, IM2NP, Marseille, France ;² Research Center for Functional Materials, National Institute for Materials Science, 1-1 Namiki, Tsukuba, Ibaraki 305-0044.

* Correspondence: marco.abbarchi@im2np.fr

Version July 31, 2020 submitted to *Nanomaterials*

Abstract: Droplet epitaxy allows the efficient fabrication of a plethora of 3D, III-V-based nanostructures on different crystalline orientations. Quantum dots grown on (311)A-oriented surface are obtained with record surface density, with or without a wetting layer. These are appealing features for quantum-dot lasing, thanks to the large density of quantum emitters and a truly 3D lateral confinement. However, the intimate photophysics of this class of nanostructures has not yet been investigated. Here we address the main optical and electronic properties of s-shell excitons in individual quantum dots grown on (311)A substrates with photoluminescence spectroscopy experiments. We show the presence of neutral exciton and biexciton as well as positive and negative charged excitons. We investigate the origins of spectral broadening, identifying them in spectral diffusion at low temperature and phonon-interaction at higher temperature, the presence of fine interactions between electron and hole spin, and a relevant heavy-hole/light-hole mixing. We interpret the level filling with a simple Poissonian model reproducing the power excitation dependence of the s-shell excitons. These results are relevant for the further improvement of this class of quantum emitters and their exploitation as single photon sources for low density samples as well as for efficient lasers for high density samples.

Keywords: III-V Quantum dots, Droplet Epitaxy, exciton dynamics, (311)A oriented substrate

1. Introduction

The continuous development of droplet epitaxy (DE)[1–3] as growth protocol for III-V-based semiconductor nanostructures enabled the fabrication of state-of-the-art devices such as lasers[4–8] and quantum emitters, including single photon sources[9–13] and entangled photons[14–17] with electrical injection[18]. The versatility of this method allowed to grow many different semiconductor alloys (GaInSb[19], AlGaAs[20–24], InGaAs[25–31] InGaP[13,32,33]), forming a plethora of nanostructures[34] such as quantum dots (QDs), multiple-concentric quantum rings[5,10,35–40], coupled structures such as ring-on-a-disk[41], dot in-a-ring[42] or dot-on-a-disk[43], as well as elongated structures such as nanowires[7]. This technique allows to independently tune size and density of the nanostructures[44] and to grow them with or without a wetting layer[7,22,26,27,45–49], aspects that are not matched by the conventional Stranski-Krastanov approach based on strain[50].

Another aspect relevant for applications is the possibility to grow high-quality nanostructures on different substrate orientation, providing the ground for highly symmetric QDs on (111)A surfaces[13, 14,22,23,28,29,33,44,51–54] (e.g. for entangled photon pairs generation) and for ultra-high density quantum wires[7] and QDs[6,19,25,46–48,55,56] formation on the highly anisotropic (311)A surface (e.g. for laser emission). This latter class of nanostructures grown on (311)A surface has not yet been

33 thoroughly investigated and a clear assessment of the corresponding excitonic dynamics has not yet
34 been reported.

35 In this paper we show a detailed structural and optical characterization of individual QDs grown
36 on the (311)A surface. We provide a clear-cut attribution of the main recombination lines observed in
37 the photoluminescence (PL) spectrum to the s-shell excitons[20,56,57] based on polarization resolved
38 PL measurements, power dependence and line broadening measurements. Neutral exciton X and
39 biexciton XX, positive X^+ and negative charged excitons X^- are characterised by the presence of fine
40 interactions[20,21,27,58] as well as by heavy-hole/light-hole mixing[59–63]. Their power dependence
41 under laser excitation above barrier is well reproduced by a simple Poissonian model that precisely
42 accounts for the main features and allows to estimate the excitonic capture volume[64]. Inhomogeneous
43 line broadening at low temperature is ascribed to spectral diffusion[11,17,65–68]induced by the
44 presence of charged defects nearby the QDs[69] and is specific of the excitonic complex in study[70,71].
45 Finally, at larger temperature, the photoluminescence of individual QDs broadens and quenches owing
46 to phonon interactions[72–74].

47 2. Materials and Methods

48 2.1. Sample fabrication

49 The sample was grown on a semi-insulating GaAs (311)A substrate by conventional solid-source
50 molecular-beam epitaxy system. After the growth of a 2 μm -thick $\text{Al}_{0.55}\text{Ga}_{0.45}\text{As}$ layer, a 136 nm-thick
51 $\text{Al}_{0.26}\text{Ga}_{0.74}\text{As}$ core-layer was grown at 610 °C. At the core-layer center GaAs QDs were formed by
52 droplet epitaxy. On the $\text{Al}_{0.26}\text{Ga}_{0.74}\text{As}$ surface, nominally 1.5 monolayers of Ga (at a growth speed of
53 about 0.1 monolayers per second) was supplied without As_4 flux at 275 °C for the droplets formation.
54 These droplets were then crystallized into GaAs QDs by supplying an As_4 flux (2×10^{-6} Torr beam
55 equivalent pressure) at 200 °C. The QDs were annealed at 400 °C for 10 min under As_4 flux supply
56 without capping in order to improve the crystal quality. After annealing, the QDs were covered with a
57 30 nm-thick $\text{Al}_{0.26}\text{Ga}_{0.74}\text{As}$ capping layer at 400 °C and the rest of the $\text{Al}_{0.26}\text{Ga}_{0.74}\text{As}$ (38 nm) layer was
58 grown at 625 °C. Once the entire growth sequence was completed, a rapid thermal annealing process
59 was performed at 785 °C for 4 min in an As_4 atmosphere to improve the optical quality.

60 2.2. Optical spectroscopy

61 The photoluminescence (PL) of individual QDs was collected with a confocal-spectroscopic setup
62 (lateral resolution about 1 μm) CW laser excitation was performed above-barrier, at 532 nm (about
63 2.3 eV). The PL is then fed into a spectrometer and detected by a Si-based CCD camera, allowing for a
64 spectral resolution better than 50 μeV in full width at half maximum (FWHM). All experiments were
65 performed in a liquid-helium cryostat between 10 and 100 K.

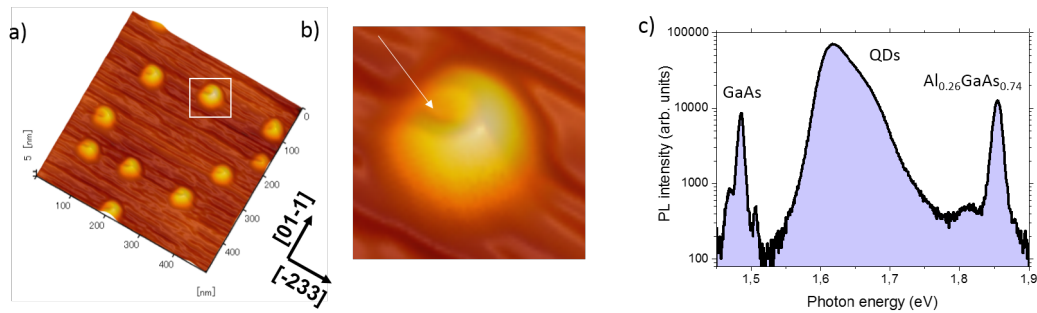
66 **3. Results and discussion**

Figure 1. (A) Atomic force microscope micrograph representing a 3D view of GaAs QDs grown on a (311)A oriented $\text{Al}_{0.26}\text{Ga}_{0.74}\text{As}$ surface. The main crystallographic axes are highlighted. (B) Blow-up of a single QD from A. The arrow highlights a hole in the QD side. (C) Photoluminescence (PL) spectrum (in semi-log scale) at 5 K showing the emission of (respectively from the low to the high energy side) the GaAs, the GaAs QDs and the $\text{Al}_{0.26}\text{Ga}_{0.74}\text{As}$ barrier layers.

67 Figure 1 A and B show atomic force micrographs (AFM) of the sample after annealing at 400 °C.
 68 Well-defined QDs are present with a density of about $5 \times 10^9/\text{cm}^2$. The QD morphology is highly
 69 asymmetric, with a U-shape (Figure 1 B). We attribute the formation mechanism of these asymmetric
 70 QDs to the low-intensity As_4 supply for the crystallization of the droplets and surface asymmetry
 71 of the (311)A surface [6,7,19,25,46–48,55]. In this growth conditions the Ga droplets crystallization
 72 into GaAs is enhanced around the edge of the droplets. In the case of standard (100) surface, in
 73 which the oppositely oriented directions of [011] and [0-11] are equivalent, ring-like structures with
 74 central holes are formed [35,36]. On the (311)A surface however, the oppositely oriented directions of
 75 [-233] and [2-3-3] are not equivalent while the directions of [01-1] and [0-11] are equivalent. Thus, the
 76 crystallization is enhanced only in a particular direction ([-233]). As the results, U-shaped QDs are
 77 formed.

78 Macro PL on the QDs ensemble taken at low temperature shows the different contributions from
 79 the GaAs substrate (at about 1.48 eV), the $\text{Al}_{0.26}\text{Ga}_{0.74}\text{As}$ barriers (at about 1.85 eV) and the QDs in
 80 between, extending over a broad band from about 1.55 eV up to 1.75 eV.

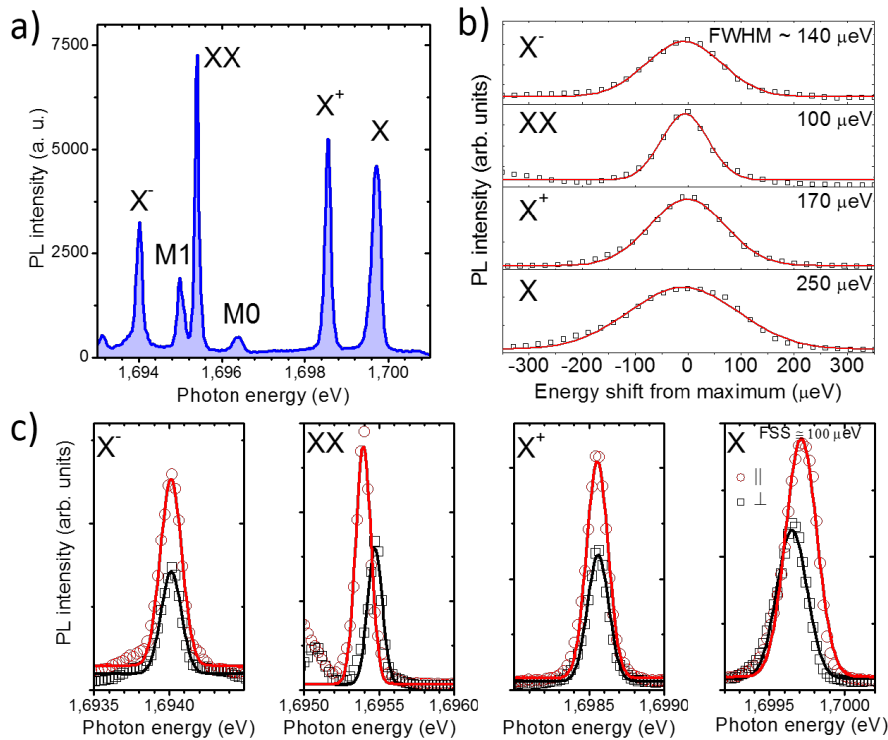
81 **4. s-shell excitons.**

Figure 2. (A) PL spectrum of a single GaAs QD sandwiched between (311)A $\text{Al}_{0.35}\text{Ga}_{0.65}\text{As}$ barrier layers. The labels on the most intense lines X, X^+ , XX and X^- highlight respectively the emission from the neutral exciton, the positive charged exciton, the neutral biexciton and the negative charged exciton. M0 and M1 highlight other non-attributed multiexciton complexes. (B) Symbols: PL spectra of X, X^+ , XX and X^- (respectively from the bottom to the top panel). Red lines are Gaussian fit to the data. The corresponding full width at half maximum (FWHM) is reported on each panel. (C) Linearly polarized components of X, X^+ , XX and X^- PL (respectively from the right to the left panel). Red and black symbols indicate orthogonal polarization. The continuous lines are Gaussians fits. The fine structure splitting (FSS) measured from the X and XX components, is about $100 \mu\text{eV}$.

82 Typical spectra of individual QDs on (311)A substrate appear structured in several sharp lines
 83 (Figure 2 A). In analogy to most III-V epitaxial QDs including those fabricated via DE[9,20,75], in the
 84 low excitation power regime the s-shell excitons dominate the PL spectrum. We ascribe the brightest
 85 lines to the recombination of the neutral exciton X (one electron, e , and a heavy-hole, hh), neutral
 86 biexciton (XX, two e and two hh), positive charged exciton (one e and two hh), and to the negative
 87 charged exciton (two e and a hh). This attribution is based on the study of the electron-hole fine
 88 interaction[20] (fine structure splitting), line broadening[65] (spectral diffusion), and level filling[64], as
 89 discussed in the following sections. Seldom, we also observe other sharp lines, as M0 and M1 (Figure 2
 90 A) that likely involve carrier recombination from the p-shell. However, a precise attribution of these
 91 lines is not possible with this set of data and goes beyond the aim of this paper.

92 **4.1. e - h spin fine interaction: fine structure splitting.**

93 A first identification of the s-shell excitons is based on the study of the fine interaction between
 94 electron and hh spin[20,21,58,76] (the fine structure splitting, FSS). At intermediate laser excitation
 95 power (at about 420 nW) all the PL components in the spectrum are well visible (Figure 2 A). At this
 96 power, by changing the polarization angle of the detected light we monitor the emission energy of the

97 PL. We observe for X and XX a mirror-symmetric energy splitting (Figure 2 C). X^+ and X^- instead, do
98 not feature any splitting.

99 This picture corresponds very well to what is commonly observed in strain-free, III-V QDs:
100 the presence of geometrical asymmetries in the confining potential breaks the invariance of the
101 hamiltonian for rotations around the vertical growth axis[20,21,24,58,61,76,77]. More precisely, *e-h*
102 spin-spin interaction for the X state lifts the degeneracy of the corresponding energy level and leads to
103 two linearly polarised PL components depending on which recombination path is radiating. The XX
104 state has overall zero spin for *e* and *hh* in the initial state and its FSS is completely determined by that
105 of the X state, towards which it relaxes. X^+ and X^- can recombine with two possible energy equivalent
106 paths and have no FSS.

107 The measured FSS in this QD is of about 100 μeV . In other QDs we measured values in between
108 30 and 140 μeV (not shown). These values are very large if compared with QDs grown on (111)
109 substrates, where the three-fold symmetry of the crystal provides a more isotropic surface diffusion
110 and a corresponding triangular or hexagonal nanostructure shape[13,14,22,23,28,29,33,44,51–54]. The
111 origin of this splitting in (311)A QDs is attributed to asymmetries in the QDs shape that is affected by
112 the anisotropy of the underlying crystal. The measured values of FSS are in line with those observed
113 in (001) QDs in spite of the larger anisotropy of the (311)A surface[20,21,58,76]. Owing to the growth
114 method in use, that allows for 3D growth of lattice-matched materials such as GaAs on AlGaAs, we
115 exclude the presence of any strain in the structure that is a major origin of symmetry breaking (and
116 thus FSS) in conventional Stranski-Krastanov III-V QDs[76].

117 4.2. Polarization intensity anisotropy: heavy-hole light-hole mixing.

118 A remarkable intensity change is visible for the two orthogonally polarized components (between
119 1/3 and 1/2, depending on the observed line, Figure 2 C)) of X and XX as well as in the polarization
120 intensity of X^+ and X^- . We ascribe this difference to heavy-hole/light-hole (*hh-lh*) mixing[59–63,78].
121 This feature was first highlighted in DE QDs grown on (001)-oriented substrates and was explained
122 as an effect of the different *hh* and *lh* bands dispersion in the different crystallographic directions[59].
123 While *e* states can be approximately described as isotropic and parabolic bands, valence *hh* and *lh*
124 bands are affected by strong anisotropy and different curvatures. In spite of the large energy splitting
125 between *hh* and *lh* bands in GaAs (tens of meV), strain and corresponding piezoelectricity[60,62,63,78]
126 (in SK QDs) or shape asymmetries[59,61] (in DE QDs) lead to a substantial mixing of the corresponding
127 *hh* and *lh* states, providing different selection rules (uneven PL intensity) for the two recombination
128 paths. Here we observe differences in the PL intensity that are of the same order of those observed in
129 the (001) counterpart[59,60,62,63,78].

130 5. Line broadening: spectral diffusion.

131 By monitoring the line-shape and corresponding broadening of each PL component in the s-shell
132 we observe respectively, a common Gaussian envelope and a remarkably different full width at half
133 maximum (FWHM, Figure 2 B). The common origin of the line broadening in this class of QDs
134 is spectral diffusion: in spite of the expected natural linewidth that should be of the order of a
135 few μeV with a corresponding Lorentian lineshape[65,67,68,75], the measured broadening values
136 (tens to hundreds of μeV) and Gaussian envelopes are the fingerprints of a fluctuating charged
137 environment. Charging and un-charging of electron and holes traps nearby the QDs (within a few tens
138 of nm), produces a variable quantum confined Stark-shift of the excitonic energy levels[11,17,65–69].
139 A PL measurement lasting for a few seconds acquires many photons emitted at slightly different
140 energy, thus providing a Gaussian lineshape. However, owing to the different *hh* and *e* confinement
141 (larger penetration in the barrier for *e* with respect to *hh*) and a screening of external electric field for
142 many-particles states, the corresponding Stark-shift can be very different. It has been routinely reported
143 a larger broadening of X with respect to the other s-shell excitons, whereas the relative broadening of
144 XX, X^+ and X^- can be very different, depending on the carrier trapped and its position with respect to

145 the QD[11,65,79]. As an example, the case in Figure 2 B seems to correspond to electrons confined in
 146 the plane of the QD[65]. However, this picture can be quite different from a QD to another, owing to
 147 the randomness and local changes of the extrinsic disorder.

148 In this samples the presence of defects in the QDs environment is likely due to the rather low
 149 temperature used to form 3D nanostructures. This is a well-known issue affecting QDs grown by
 150 droplet epitaxy. However, in principle it could be overcome as it has been shown for droplet epitaxial
 151 QDs grown on other surface orientations[14,66].

152 6. Power dependence: level filling.

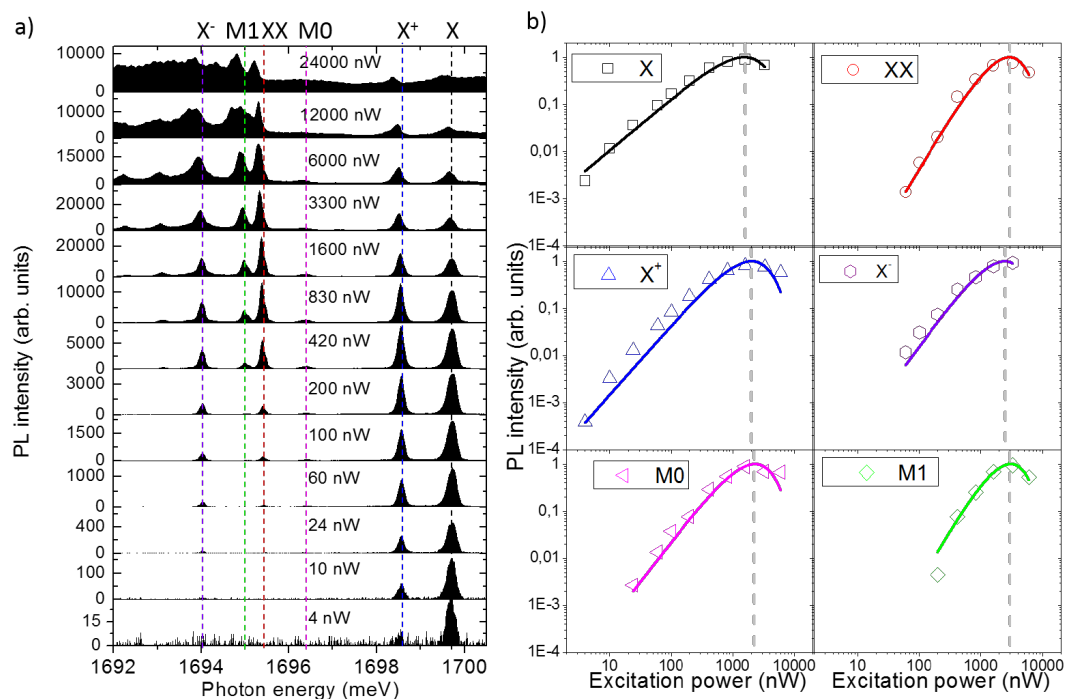


Figure 3. (A) PL spectra from low to high excitation power for the same QD shown in Fig. 2. The incident power is highlighted on each panel. The vertical dashed lines are guides to the eyes. (B) Evolution of the six main PL lines as a function of the incident excitation power. The PL intensity has been normalized to the maximum for each component. Each panel refers to a specific exciton complex recombination as highlighted by the corresponding labels. Symbols are the experimental data whereas lines are Poissonian fits.

153 A typical evolution of the PL spectrum of an individual QD as a function of the incident power is
 154 provided in Figure 3 A. At low power only two lines, X and X⁺ are visible with a dominant intensity
 155 of X, while when increasing the power also X⁻ and, soon after, XX appear. At larger power X and X⁺
 156 swap their relative intensity and then quench. XX and X⁻ reach their maximum and quench at very
 157 large power. M0 and M1 follows a similar dynamics of X⁻ and XX, respectively. At lower energy, other
 158 peaks appear together with a broad background that then extends to all the spectrum. These latter
 159 features are interpreted as the effect of multi-excitons recombining from the p-shell and the coupling
 160 with the continuum of states above the confined energy levels. For the sake of thoroughness, we note a
 161 slight red-shift of the PL intensity at large excitation power. This effect is interpreted as a heating of
 162 the sample. It is also worth noting that the PL intensity of the s-shell excitons can be followed over
 163 more than 3 order of magnitude of the excitation power, meaning that the capture and recombination
 164 processes are very efficient in this sample.

165 A simple but meaningful description of the level filling of individual QDs can be provided by
 166 a model based on the assumption that carrier capture and recombination are random processes[80].
 167 By assuming an infinite set of confined levels in the nanostructure, that obviously constitutes a rough
 168 approximation, the model can be further simplified to a Poissonian dependence of the PL intensity[64,
 169 80]. In spite of its simplicity, this modeling accounts extremely well for power dependence[64] and
 170 recombination dynamics[33,81] of the s-shell excitons. In this model we assume that the PL intensity
 171 I_{PL} of a given energy level is proportional to the occupation probability N_n of that level:

$$I_{PL} \propto N_n \quad (1)$$

172
 173 The Poissonian model for level filling predicts that the occupation of a certain level with n excitons
 174 N_n is provided by:

$$N_n = \frac{\langle n \rangle^n}{n!} e^{-\langle n \rangle} \quad (2)$$

175
 176 Thus, for $n = 1$ N_1 describes the level filling of X, for $n = 2$ N_2 describes the level filling of XX,
 177 etc. $\langle n \rangle$ is the average number of exciton created in the QD. This number is obtained averaging
 178 over many capture/recombination cycles and under steady state excitation and is defined as $\langle n \rangle =$
 179 $N_R \tau_r / \tau_c$, with N_R is the number of e-h pairs created in the reservoir, τ_r is the exciton recombination
 180 rate and τ_c the exciton capture rate. Provided that τ_r and τ_c lie in the ps to ns range and the integration
 181 time for a PL measurement last about one second, this hypothesis is well satisfied.

182 A final phenomenological assumption for $\langle n \rangle$ that allows to link the experimental data to this
 183 Poissonian model is that

$$\langle n \rangle = \beta F_{exc}^\alpha \quad (3)$$

184
 185 where α and β are constants characterising the capture mechanism. Note that in the vast majority
 186 of works on QDs, the level filling of the s-shell excitons is simply provided by equation 3, with
 187 $\alpha(X) \sim 1$ for X, and $\alpha(XX) \sim 2$ for XX. However, this over-simplified assumption does not account
 188 for saturation and quenching of the PL lines under CW excitation[18,20,52,82].

189 The Poissonian model well reproduces the power dependence of X and XX that are extracted by
 190 integrating in energy their PL line up to 1600 nW after background subtraction (3 B). Fitting the data
 191 using Equation 2 and 3 we obtain $\alpha_X = 1.1$ (very close to 1 as expected) and a simultaneous fit of X
 192 and XX with the same parameters. Saturation power of X is about 1500 nW and about two times larger
 193 for XX.

194 Although the simple Poissonian model allows only for neutral excitons capture ($n = 1, 2, \dots$)
 195 and in principle cannot account for charged complexes, a nice fitting of the data can be recovered by
 196 assuming half-integer numbers[64]. In this case the model is modified by adding a phenomenological
 197 coefficient γ to α_X modifying as follows:

$$N_n = \frac{(\langle n \rangle^n)^\gamma}{n!} e^{-\langle n \rangle} \quad (4)$$

198
 199 thus, for instance $\gamma = 1$ corresponds to the neutral exciton X state whereas $\gamma = 1.5$ is *one and an*
 200 *half exciton* (between X and XX), that is a charged exciton. By using Equation 4 we can nicely fit the
 201 power dependence of X^+ and X^- by keeping unchanged the parameters α and β that were used to fit
 202 X and XX (3 B). We obtain $\alpha(X^+) = 1.3\alpha(X)$ and $\alpha(X^-) = 1.6\alpha(X)$ that are very close to 1.5. Finally,
 203 we note that also the dynamics of M0 and M1 with incident power can be nicely accounted for by this
 204 pseudo-Poissonian model providing $\alpha(M0) = 1.5\alpha(X)$ and $\alpha(M1) = 2.1\alpha(X)$. These values of γ larger

205 than 1 account for the super-linear dependence on the incident power and suggest a multi-exciton
 206 nature of these energy levels.

207 To conclude this section we estimate the QD capture volume for excitons[64]. This can be deduced
 208 from the saturation power of the X level: at that power (of about 1500 nW distributed over a diameter
 209 of 1 μm) the number of carriers created in the host matrix around the QD provides a steady occupation
 210 of the X level by one exciton. Thus, the inverse of the carrier density injected in the semiconductor at
 211 that saturation power represents the capture volume. Assuming a penetration depth of the laser light
 212 of about 1 μm , an excitonic recombination lifetime of about 1 ns and considering the QD as a sphere,
 213 we can roughly deduce a capture radius of the order of 50 nm. This value is rather larger than the
 214 physical size of the QD, that is of the order of a few nm. We also observe that this value is perfectly in
 215 line with those measured in the (001) DE QDs counterpart[64] as well as in other kind of quantum
 216 emitters in III-V[79] and in group IV materials[83].

217 6.1. Temperature dependence.

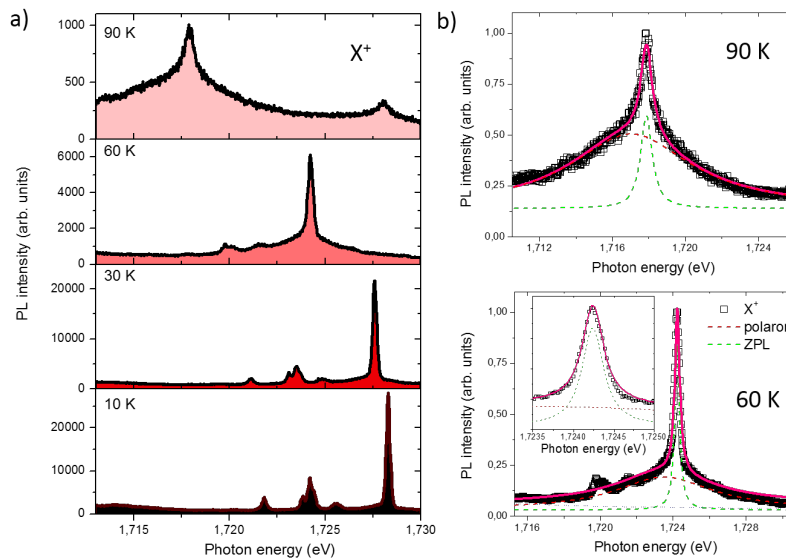


Figure 4. (A) Selected PL spectra from 10 to 90 K of a single QD with a bright X^+ emission. (B) Bottom panel: detail of the spectrum from A at 60 K with Lorentzian fits of the zero phonon line and the polaron band. The inset shows a blow up of the ZPL. Top panel: detail of the spectrum at 90 K with Lorentzian fits.

218 Bright PL emission can be observed well above liquid nitrogen temperature (Figure 4). A quadratic
 219 red-shift of the exciton emission is observed, as expected for this class of nanostructures that follows
 220 the empirical Varshni law (Figure 4 A). At the same time, a strong quenching of the PL intensity of
 221 about two orders of magnitude is observed when passing from 10 to 90 K.

222 The low-temperature spectrum (up to about 30 K), as discussed in the previous sections, shows
 223 sharp lines attributed to the s-shell excitons and is well described by a Gaussian envelope (Figure 2)[65].
 224 At higher temperature instead, when the phonon population plays an important role, we observe
 225 the onset of a broad Lorentzian-shaped pedestal below the original sharp line that can be now well
 226 approximated with a Lorentzian envelope (Figure 4 B)[72,73,84]. The relative intensity of this broad
 227 pedestal increases up to dominate over the sharp central line. This phenomenology corresponds well
 228 to what has been thoroughly explained by using the Huang-Rhys formalism for (001) DE QDs as well
 229 as for SK QDs[72,73,84]: the broad band is interpreted as a superposition of acoustic phonon replicas
 230 (polaron) whereas the sharp central line emission is assigned to the zero phonon line (ZPL).

7. Conclusions

In conclusion we showed that droplet epitaxial QDs grown on the highly anisotropic (311)A surface are characterised by bright PL lines emitting at visible frequency. These lines correspond well to the picture of s-shell excitons recombination in III-V nanostructures. We measured a relatively large fine structure splitting (10-100 μeV) of the neutral exciton X, that is justified by the anisotropic shape of these QDs. Inhomogeneous line broadening lies in the 100 μeV and is ascribed to spectral diffusion originating from the fluctuating charged environment. This broadening is specific of each excitonic species and reflects the nature and position of the trapped carriers. Level filling of the s-shell excitons is well accounted for by a simple Poissonian model that allows to describe the power dependence of the main PL lines and to estimate an excitonic capture volume much larger than the physical size of the QD. Finally, a bright PL emission is still visible well above liquid nitrogen temperature.

Overall, these results account for the high quality and brightness of this class of QDs where X, XX and X⁺ emission can be followed for about 3 orders of magnitude of excitation power below saturation and up to relatively large temperature that are appealing features for applications as single photon sources. The low-temperature linewidth is rather large with respect to state-of-the-art droplet epitaxial quantum dots and in principle it could be improved by using alternative fabrication processes at higher temperature.

Funding:

Acknowledgments:

Conflicts of Interest: The authors declare no conflict of interest.

Abbreviations

The following abbreviations are used in this manuscript:

PL	photoluminescence
QD	quantum dot
FSS	fine structure splitting
X	neutral exciton
X ⁺	positive charged exciton
XX	neutral biexciton
X ⁻	negative charged exciton
FWHM	full width at half maximum

- Mantovani, V.; Sanguinetti, S.; Guzzi, M.; Grilli, E.; Gurioli, M.; Watanabe, K.; Koguchi, N. Low density GaAs/ AlGaAs quantum dots grown by modified droplet epitaxy. *Journal of applied physics* **2004**, *96*, 4416–4420.
- Wu, J.; Wang, Z.M. Droplet epitaxy for advanced optoelectronic materials and devices. *Journal of Physics D: Applied Physics* **2014**, *47*, 173001.
- Gurioli, M.; Wang, Z.; Rastelli, A.; Kuroda, T.; Sanguinetti, S. Droplet epitaxy of semiconductor nanostructures for quantum photonic devices. *Nature materials* **2019**, p. 1.
- Mano, T.; Kuroda, T.; Yamagiwa, M.; Kido, G.; Sakoda, K.; Koguchi, N. Lasing in Ga As/ Al Ga As self-assembled quantum dots. *Applied physics letters* **2006**, *89*, 183102.
- Mano, T.; Kuroda, T.; Mitsuishi, K.; Yamagiwa, M.; Guo, X.J.; Furuya, K.; Sakoda, K.; Koguchi, N. Ring-shaped GaAs quantum dot laser grown by droplet epitaxy: effects of post-growth annealing on structural and optical properties. *Journal of crystal growth* **2007**, *301*, 740–743.
- Mano, T.; Kuroda, T.; Mitsuishi, K.; Nakayama, Y.; Noda, T.; Sakoda, K. Ga As/ Al Ga As quantum dot laser fabricated on GaAs (311) A substrate by droplet epitaxy. *Applied Physics Letters* **2008**, *93*, 203110.
- Jo, M.; Keizer, J.G.; Mano, T.; Koenraad, P.M.; Sakoda, K. Self-assembly of GaAs quantum wires grown on (311) A substrates by droplet epitaxy. *Applied physics express* **2011**, *4*, 055501.

- 272 8. Jo, M.; Mano, T.; Sakoda, K. Electrical Lasing in GaAs Quantum Dots Grown by Droplet Epitaxy. *Advances*
273 *in Optical Materials*. Optical Society of America, 2012, pp. ITh5B–6.
- 274 9. Kuroda, T.; Abbarchi, M.; Mano, T.; Watanabe, K.; Yamagiwa, M.; Kuroda, K.; Sakoda, K.; Kido, G.;
275 Koguchi, N.; Mastrandrea, C.; others. Photon correlation in GaAs self-assembled quantum dots. *Applied*
276 *physics express* **2008**, *1*, 042001.
- 277 10. Abbarchi, M.; Mastrandrea, C.; Vinattieri, A.; Sanguinetti, S.; Mano, T.; Kuroda, T.; Koguchi, N.; Sakoda, K.;
278 Gurioli, M. Photon antibunching in double quantum ring structures. *Physical Review B* **2009**, *79*, 085308.
- 279 11. Abbarchi, M.; Kuroda, T.; Mano, T.; Gurioli, M.; Sakoda, K. Bunched photon statistics of the spectrally
280 diffusive photoluminescence of single self-assembled GaAs quantum dots. *Physical Review B* **2012**,
281 *86*, 115330.
- 282 12. Benyoucef, M.; Zuerbig, V.; Reithmaier, J.P.; Kroh, T.; Schell, A.W.; Aichele, T.; Benson, O. Single-photon
283 emission from single InGaAs/GaAs quantum dots grown by droplet epitaxy at high substrate temperature.
284 *Nanoscale research letters* **2012**, *7*, 1–5.
- 285 13. Kumano, H.; Harada, T.; Suemune, I.; Nakajima, H.; Kuroda, T.; Mano, T.; Sakoda, K.; Odashima, S.;
286 Sasakura, H. Stable and efficient collection of single photons emitted from a semiconductor quantum dot
287 into a single-mode optical fiber. *Applied Physics Express* **2016**, *9*, 032801.
- 288 14. Kuroda, T.; Mano, T.; Ha, N.; Nakajima, H.; Kumano, H.; Urbaszek, B.; Jo, M.; Abbarchi, M.; Sakuma, Y.;
289 Sakoda, K.; others. Symmetric quantum dots as efficient sources of highly entangled photons: Violation of
290 Bell's inequality without spectral and temporal filtering. *Physical Review B* **2013**, *88*, 041306.
- 291 15. Kumano, H.; Nakajima, H.; Kuroda, T.; Mano, T.; Sakoda, K.; Suemune, I. Nonlocal biphoton generation in
292 a Werner state from a single semiconductor quantum dot. *Physical review B* **2015**, *91*, 205437.
- 293 16. Basso Basset, F.; Bietti, S.; Reindl, M.; Esposito, L.; Fedorov, A.; Huber, D.; Rastelli, A.; Bonera, E.; Trotta, R.;
294 Sanguinetti, S. High-yield fabrication of entangled photon emitters for hybrid quantum networking using
295 high-temperature droplet epitaxy. *Nano letters* **2018**, *18*, 505–512.
- 296 17. Ramírez, H.Y.; Chou, Y.L.; Cheng, S.J. Effects of electrostatic environment on the electrically triggered
297 production of entangled photon pairs from droplet epitaxial quantum dots. *Scientific reports* **2019**, *9*, 1–10.
- 298 18. Ha, N.; Mano, T.; Kuroda, T.; Sakuma, Y.; Sakoda, K. Current-injection quantum-entangled-pair emitter
299 using droplet epitaxial quantum dots on GaAs (111) A. *Applied Physics Letters* **2019**, *115*, 083106.
- 300 19. Kawazu, T.; Noda, T.; Mano, T.; Jo, M.; Sakaki, H. Effects of antimony flux on morphology and
301 photoluminescence spectra of GaSb quantum dots formed on GaAs by droplet epitaxy. *Journal of Nonlinear*
302 *Optical Physics & Materials* **2010**, *19*, 819–826.
- 303 20. Abbarchi, M.; Mastrandrea, C.; Kuroda, T.; Mano, T.; Sakoda, K.; Koguchi, N.; Sanguinetti, S.; Vinattieri, A.;
304 Gurioli, M. Exciton fine structure in strain-free GaAs/Al 0.3 Ga 0.7 As quantum dots: Extrinsic effects.
305 *Physical Review B* **2008**, *78*, 125321.
- 306 21. Plumhof, J.; Křápek, V.; Wang, L.; Schliwa, A.; Bimberg, D.; Rastelli, A.; Schmidt, O. Experimental
307 investigation and modeling of the fine structure splitting of neutral excitons in strain-free GaAs/Al x Ga 1-
308 x As quantum dots. *Physical Review B* **2010**, *81*, 121309.
- 309 22. Mano, T.; Abbarchi, M.; Kuroda, T.; McSkimming, B.; Ohtake, A.; Mitsuishi, K.; Sakoda, K. Self-assembly
310 of symmetric GaAs quantum dots on (111) A substrates: Suppression of fine-structure splitting. *Applied*
311 *physics express* **2010**, *3*, 065203.
- 312 23. Bouet, L.; Vidal, M.; Mano, T.; Ha, N.; Kuroda, T.; Durnev, M.; Glazov, M.; Ivchenko, E.; Marie, X.; Amand,
313 T.; others. Charge tuning in [111] grown GaAs droplet quantum dots. *Applied Physics Letters* **2014**,
314 *105*, 082111.
- 315 24. Yeo, I.; Kim, D.; Lee, K.T.; Kim, J.S.; Song, J.D.; Park, C.H.; Han, I.K. Comparative Chemico-Physical
316 Analyses of Strain-Free GaAs/Al_{0.3}Ga_{0.7}As Quantum Dots Grown by Droplet Epitaxy. *Nanomaterials*
317 **2020**, *10*, 1301.
- 318 25. Saidi, F.; Bouzaiene, L.; Sfaxi, L.; Maaref, H. Growth conditions effects on optical properties of InAs
319 quantum dots grown by molecular beam epitaxy on GaAs (1 1 3) A substrate. *Journal of luminescence* **2012**,
320 *132*, 289–292.
- 321 26. Zuerbig, V.; Bugaew, N.; Reithmaier, J.P.; Kozub, M.; Musiał, A.; Sęk, G.; Misiewicz, J. Growth-Temperature
322 Dependence of Wetting Layer Formation in High Density InGaAs/GaAs Quantum Dot Structures Grown
323 by Droplet Epitaxy. *Japanese Journal of Applied Physics* **2012**, *51*, 085501.

- 324 27. Skiba-Szymanska, J.; Stevenson, R.M.; Varnava, C.; Felle, M.; Huwer, J.; Müller, T.; Bennett, A.J.; Lee, J.P.;
325 Farrer, I.; Krysa, A.B.; others. Universal growth scheme for quantum dots with low fine-structure splitting
326 at various emission wavelengths. *Physical Review Applied* **2017**, *8*, 014013.
- 327 28. Mano, T.; Mitsuishi, K.; Ha, N.; Ohtake, A.; Castellano, A.; Sanguinetti, S.; Noda, T.; Sakuma, Y.; Kuroda, T.;
328 Sakoda, K. Growth of metamorphic InGaAs on GaAs (111) a: counteracting lattice mismatch by inserting a
329 thin InAs interlayer. *Crystal Growth & Design* **2016**, *16*, 5412–5417.
- 330 29. Ha, N.; Mano, T.; Wu, Y.N.; Ou, Y.W.; Cheng, S.J.; Sakuma, Y.; Sakoda, K.; Kuroda, T. Wavelength extension
331 beyond 1.5 μm in symmetric InAs quantum dots grown on InP (111) A using droplet epitaxy. *Applied*
332 *Physics Express* **2016**, *9*, 101201.
- 333 30. Fuster, D.; Abderrafi, K.; Alén, B.; González, Y.; Wewior, L.; González, L. InAs nanostructures grown by
334 droplet epitaxy directly on InP (001) substrates. *Journal of Crystal Growth* **2016**, *434*, 81–87.
- 335 31. Sala, E.M.; Na, Y.I.; Godsland, M.; Trapalis, A.; Heffernan, J. InAs/InP Quantum Dots in Etched
336 Pits by Droplet Epitaxy in Metalorganic Vapor Phase Epitaxy. *physica status solidi (RRL) – Rapid*
337 *Research Letters* **2020**, *n/a*, 2000173, [<https://onlinelibrary.wiley.com/doi/pdf/10.1002/pssr.202000173>].
338 doi:10.1002/pssr.202000173.
- 339 32. Prongjit, P.; Ratanathammaphan, S.; Ha, N.; Mano, T.; Sakoda, K.; Kuroda, T. Type-II recombination
340 dynamics of tensile-strained GaP quantum dots in GaAs grown by droplet epitaxy. *Applied Physics Letters*
341 **2016**, *109*, 171902.
- 342 33. Ha, N.; Mano, T.; Dubos, S.; Kuroda, T.; Sakuma, Y.; Sakoda, K. Single photon emission from droplet
343 epitaxial quantum dots in the standard telecom window around a wavelength of 1.55 μm . *Applied Physics*
344 *Express* **2020**, *13*, 025002.
- 345 34. Bietti, S.; Bocquel, J.; Adorno, S.; Mano, T.; Keizer, J.G.; Koenraad, P.M.; Sanguinetti, S. Precise shape
346 engineering of epitaxial quantum dots by growth kinetics. *Physical Review B* **2015**, *92*, 075425.
- 347 35. Mano, T.; Koguchi, N. Nanometer-scale GaAs ring structure grown by droplet epitaxy. *Journal of crystal*
348 *growth* **2005**, *278*, 108–112.
- 349 36. Mano, T.; Kuroda, T.; Sanguinetti, S.; Ochiai, T.; Tateno, T.; Kim, J.; Noda, T.; Kawabe, M.; Sakoda, K.; Kido,
350 G.; others. Self-assembly of concentric quantum double rings. *Nano letters* **2005**, *5*, 425–428.
- 351 37. Somaschini, C.; Bietti, S.; Koguchi, N.; Sanguinetti, S. Fabrication of multiple concentric nanoring structures.
352 *Nano letters* **2009**, *9*, 3419–3424.
- 353 38. Shwartz, N.L.; Vasilenko, M.A.; Nastovjak, A.G.; Neizvestny, I.G. Concentric GaAs nanorings formation
354 by droplet epitaxy—Monte Carlo simulation. *Computational Materials Science* **2018**, *141*, 91–100.
- 355 39. Sanguinetti, S.; Mano, T.; Kuroda, T. Self-assembled semiconductor quantum ring complexes by droplet
356 epitaxy: growth and physical properties. In *Physics of Quantum Rings*; Springer, 2018; pp. 187–228.
- 357 40. Heyn, C.; Zocher, M.; Hansen, W. Functionalization of Droplet Etching for Quantum Rings. In *Physics of*
358 *Quantum Rings*; Springer, 2018; pp. 139–162.
- 359 41. Somaschini, C.; Bietti, S.; Sanguinetti, S.; Koguchi, N.; Fedorov, A. Self-assembled GaAs/AlGaAs coupled
360 quantum ring-disk structures by droplet epitaxy. *Nanotechnology* **2010**, *21*, 125601.
- 361 42. Somaschini, C.; Bietti, S.; Koguchi, N.; Sanguinetti, S. Coupled quantum dot–ring structures by droplet
362 epitaxy. *Nanotechnology* **2011**, *22*, 185602.
- 363 43. Elborg, M.; Noda, T.; Mano, T.; Kuroda, T.; Yao, Y.; Sakuma, Y.; Sakoda, K. Self-assembly of vertically
364 aligned quantum ring-dot structure by Multiple Droplet Epitaxy. *Journal of Crystal Growth* **2017**,
365 *477*, 239–242.
- 366 44. Ohtake, A.; Ha, N.; Mano, T. Extremely high-and low-density of Ga droplets on GaAs {111} A, B:
367 Surface-polarity dependence. *Crystal Growth & Design* **2015**, *15*, 485–488.
- 368 45. Sanguinetti, S.; Watanabe, K.; Tateno, T.; Wakaki, M.; Koguchi, N.; Kuroda, T.; Minami, F.; Gurioli, M. Role
369 of the wetting layer in the carrier relaxation in quantum dots. *Applied physics letters* **2002**, *81*, 613–615.
- 370 46. Mano, T.; Noda, T.; Kuroda, T.; Sanguinetti, S.; Sakoda, K. Self-assembled GaAs quantum dots coupled
371 with GaAs wetting layer grown on GaAs (311) A by droplet epitaxy. *physica status solidi c* **2011**, *8*, 257–259.
- 372 47. Keizer, J.; Jo, M.; Mano, T.; Noda, T.; Sakoda, K.; Koenraad, P. Structural atomic-scale analysis of
373 GaAs/AlGaAs quantum wires and quantum dots grown by droplet epitaxy on a (311) A substrate. *Applied*
374 *Physics Letters* **2011**, *98*, 193112.

- 375 48. Keizer, J.; Koenraad, P. Atomic-scale analysis of self-assembled quantum dots by cross-sectional scanning,
376 tunneling microscopy, and atom probe tomography. In *Quantum Dots: Optics, Electron Transport and Future*
377 *Applications*; Cambridge University Press, 2012; pp. 41–60.
- 378 49. Shahzadeh, M.; Sabaeian, M. Wetting layer-assisted modification of in-plane-polarized transitions in
379 strain-free GaAs/AlGaAs quantum dots. *Superlattices and Microstructures* **2014**, *75*, 514–522.
- 380 50. Sautter, K.E.; Vallejo, K.D.; Simmonds, P.J. Strain-driven quantum dot self-assembly by molecular beam
381 epitaxy. *Journal of Applied Physics* **2020**, *128*, 031101.
- 382 51. Jo, M.; Mano, T.; Abbarchi, M.; Kuroda, T.; Sakuma, Y.; Sakoda, K. Self-limiting growth of hexagonal and
383 triangular quantum dots on (111) A. *Crystal growth & design* **2012**, *12*, 1411–1415.
- 384 52. Liu, X.; Ha, N.; Nakajima, H.; Mano, T.; Kuroda, T.; Urbaszek, B.; Kumano, H.; Suemune, I.; Sakuma, Y.;
385 Sakoda, K. Vanishing fine-structure splittings in telecommunication-wavelength quantum dots grown on
386 (111) A surfaces by droplet epitaxy. *Physical Review B* **2014**, *90*, 081301.
- 387 53. Trapp, A.; Reuter, D. Formation of self-assembled GaAs quantum dots via droplet epitaxy on misoriented
388 GaAs (111) B substrates. *Journal of Vacuum Science & Technology B, Nanotechnology and Microelectronics:*
389 *Materials, Processing, Measurement, and Phenomena* **2018**, *36*, 02D106.
- 390 54. Bietti, S.; Basset, F.B.; Tuktamyshev, A.; Bonera, E.; Fedorov, A.; Sanguinetti, S. High-temperature droplet
391 epitaxy of symmetric GaAs/AlGaAs quantum dots. *Scientific Reports* **2020**, *10*, 1–10.
- 392 55. Mano, T.; Kuroda, T.; Mitsuishi, K.; Noda, T.; Sakoda, K. High-density GaAs/AlGaAs quantum dots
393 formed on GaAs (3 1 1) A substrates by droplet epitaxy. *Journal of crystal growth* **2009**, *311*, 1828–1831.
- 394 56. Abbarchi, M.; Kuroda, T.; Mano, T.; Sakoda, K.; Mastrandrea, C.A.; Vinattieri, A.; Gurioli, M.; Tsuchiya, T.
395 Energy renormalization of exciton complexes in GaAs quantum dots. *Physical Review B* **2010**, *82*, 201301.
- 396 57. Accanto, N.; Minari, S.; Cavigli, L.; Bietti, S.; Isella, G.; Vinattieri, A.; Sanguinetti, S.; Gurioli, M. Kinetics of
397 multiexciton complex in GaAs quantum dots on Si. *Applied Physics Letters* **2013**, *102*, 053109.
- 398 58. Tong, H.; Wu, M. Theory of excitons in cubic III-V semiconductor GaAs, InAs and GaN quantum dots:
399 fine structure and spin relaxation. *Physical Review B* **2011**, *83*, 235323.
- 400 59. Belhadj, T.; Amand, T.; Kunold, A.; Simon, C.M.; Kuroda, T.; Abbarchi, M.; Mano, T.; Sakoda, K.; Kunz, S.;
401 Marie, X.; others. Impact of heavy hole-light hole coupling on optical selection rules in GaAs quantum
402 dots. *Applied Physics Letters* **2010**, *97*, 051111.
- 403 60. Lin, C.H.; You, W.T.; Chou, H.Y.; Cheng, S.J.; Lin, S.D.; Chang, W.H. Anticorrelation between the splitting
404 and polarization of the exciton fine structure in single self-assembled InAs/GaAs quantum dots. *Physical*
405 *Review B* **2011**, *83*, 075317.
- 406 61. Liao, Y.H.; Liao, C.C.; Ku, C.H.; Chang, Y.C.; Cheng, S.J.; Jo, M.; Kuroda, T.; Mano, T.; Abbarchi, M.; Sakoda,
407 K. Geometrical impact on the optical polarization of droplet epitaxial quantum dots. *Physical Review B*
408 **2012**, *86*, 115323.
- 409 62. Plumhof, J.; Trotta, R.; Krápek, V.; Zallo, E.; Atkinson, P.; Kumar, S.; Rastelli, A.; Schmidt, O.G. Tuning of
410 the valence band mixing of excitons confined in GaAs/AlGaAs quantum dots via piezoelectric-induced
411 anisotropic strain. *Physical Review B* **2013**, *87*, 075311.
- 412 63. Luo, J.W.; Bester, G.; Zunger, A. Supercoupling between heavy-hole and light-hole states in nanostructures.
413 *Physical Review B* **2015**, *92*, 165301.
- 414 64. Abbarchi, M.; Mastrandrea, C.; Kuroda, T.; Mano, T.; Vinattieri, A.; Sakoda, K.; Gurioli, M. Poissonian
415 statistics of excitonic complexes in quantum dots. *Journal of Applied Physics* **2009**, *106*, 053504.
- 416 65. Abbarchi, M.; Troiani, F.; Mastrandrea, C.; Goldoni, G.; Kuroda, T.; Mano, T.; Sakoda, K.; Koguchi, N.;
417 Sanguinetti, S.; Vinattieri, A.; others. Spectral diffusion and line broadening in single self-assembled Ga
418 As/ Al Ga As quantum dot photoluminescence. *Applied physics letters* **2008**, *93*, 162101.
- 419 66. Mano, T.; Abbarchi, M.; Kuroda, T.; Mastrandrea, C.; Vinattieri, A.; Sanguinetti, S.; Sakoda, K.; Gurioli,
420 M. Ultra-narrow emission from single GaAs self-assembled quantum dots grown by droplet epitaxy.
421 *Nanotechnology* **2009**, *20*, 395601.
- 422 67. Kuroda, K.; Kuroda, T.; Watanabe, K.; Mano, T.; Kido, G.; Koguchi, N.; Sakoda, K. Distribution of exciton
423 emission linewidth observed for GaAs quantum dots grown by droplet epitaxy. *Journal of luminescence*
424 **2010**, *130*, 2390–2393.
- 425 68. Nguyen, H.S.; Sallen, G.; Abbarchi, M.; Ferreira, R.; Voisin, C.; Roussignol, P.; Cassabois, G.; Diederichs,
426 C. Photoneutralization and slow capture of carriers in quantum dots probed by resonant excitation
427 spectroscopy. *Physical review B* **2013**, *87*, 115305.

- 428 69. Ha, N.; Mano, T.; Chou, Y.L.; Wu, Y.N.; Cheng, S.J.; Bocquel, J.; Koenraad, P.M.; Ohtake, A.; Sakuma, Y.;
429 Sakoda, K.; others. Size-dependent line broadening in the emission spectra of single GaAs quantum dots:
430 Impact of surface charge on spectral diffusion. *Physical Review B* **2015**, *92*, 075306.
- 431 70. Schimpf, C.; Reindl, M.; Klenovsky, P.; Fromherz, T.; Da Silva, S.F.C.; Hofer, J.; Schneider, C.; Höfling, S.;
432 Trotta, R.; Rastelli, A. Resolving the temporal evolution of line broadening in single quantum emitters.
433 *Optics Express* **2019**, *27*, 35290–35307.
- 434 71. Reigie, A.; Hostein, R.; Voliotis, V. Resonance fluorescence of a single semiconductor quantum dot: the
435 impact of a fluctuating electrostatic environment. *Semiconductor Science and Technology* **2019**, *34*, 113001.
- 436 72. Sanguinetti, S.; Mano, T.; Oshima, M.; Tateno, T.; Wakaki, M.; Koguchi, N. Temperature dependence of the
437 photoluminescence of InGaAs/GaAs quantum dot structures without wetting layer. *Applied physics letters*
438 **2002**, *81*, 3067–3069.
- 439 73. Abbarchi, M.; Gurioli, M.; Vinattieri, A.; Sanguinetti, S.; Bonfanti, M.; Mano, T.; Watanabe, K.; Kuroda, T.;
440 Koguchi, N. Phonon sideband recombination kinetics in single quantum dots. *Journal of applied physics*
441 **2008**, *104*, 023504.
- 442 74. Lee, S.e.; Yeo, I.; Jo, M.K.; Jeong, Y.W.; Kim, T.G.; Kim, J.S.; Yi, K.S.; Han, I.K.; Song, J.D. Exciton-phonon
443 coupling channels in a ‘strain-free’ GaAs droplet epitaxy single quantum dot. *Current Applied Physics* **2018**,
444 *18*, 829–833.
- 445 75. Abbarchi, M.; Kuroda, T.; Duval, R.; Mano, T.; Sakoda, K. Scanning Fabry-Pérot interferometer with largely
446 tuneable free spectral range for high resolution spectroscopy of single quantum dots. *Review of Scientific*
447 *Instruments* **2011**, *82*, 073103.
- 448 76. Trotta, R.; Zallo, E.; Ortix, C.; Atkinson, P.; Plumhof, J.; Van den Brink, J.; Rastelli, A.; Schmidt, O. Universal
449 recovery of the energy-level degeneracy of bright excitons in InGaAs quantum dots without a structure
450 symmetry. *Physical review letters* **2012**, *109*, 147401.
- 451 77. Adorno, S.; Bietti, S.; Sanguinetti, S. Annealing induced anisotropy in GaAs/AlGaAs quantum dots grown
452 by droplet epitaxy. *Journal of crystal growth* **2013**, *378*, 515–518.
- 453 78. Fras, F.; Bernardot, F.; Eble, B.; Bernard, M.; Siarry, B.; Miard, A.; Lemaitre, A.; Testelin, C.; Chamarro, M.
454 The role of heavy–light-hole mixing on the optical initialization of hole spin in InAs quantum dots. *Journal*
455 *of Physics: Condensed Matter* **2013**, *25*, 202202.
- 456 79. Dotti, N.; Sarti, F.; Bietti, S.; Azarov, A.; Kuznetsov, A.; Biccari, F.; Vinattieri, A.; Sanguinetti, S.; Abbarchi,
457 M.; Gurioli, M. Germanium-based quantum emitters towards a time-reordering entanglement scheme
458 with degenerate exciton and biexciton states. *Physical Review B* **2015**, *91*, 205316.
- 459 80. Grundmann, M.; Bimberg, D. Theory of random population for quantum dots. *Physical Review B* **1997**,
460 *55*, 9740.
- 461 81. Kuroda, T.; Belhadj, T.; Abbarchi, M.; Mastrandrea, C.; Gurioli, M.; Mano, T.; Ikeda, N.; Sugimoto, Y.;
462 Asakawa, K.; Koguchi, N.; others. Bunching visibility for correlated photons from single GaAs quantum
463 dots. *Physical Review B* **2009**, *79*, 035330.
- 464 82. Tighineanu, P.; Daveau, R.; Lee, E.H.; Song, J.D.; Stobbe, S.; Lodahl, P. Decay dynamics and exciton
465 localization in large GaAs quantum dots grown by droplet epitaxy. *Physical Review B* **2013**, *88*, 155320.
- 466 83. Beaufiles, C.; Redjem, W.; Rousseau, E.; Jacques, V.; Kuznetsov, A.Y.; Raynaud, C.; Voisin, C.; Benali, A.;
467 Herzig, T.; Pezzagna, S.; others. Optical properties of an ensemble of G-centers in silicon. *Physical Review B*
468 **2018**, *97*, 035303.
- 469 84. Favero, I.; Cassabois, G.; Ferreira, R.; Darson, D.; Voisin, C.; Tignon, J.; Delalande, C.; Bastard, G.;
470 Roussignol, P.; Gérard, J. Acoustic phonon sidebands in the emission line of single InAs/GaAs quantum
471 dots. *Physical Review B* **2003**, *68*, 233301.